Creating Polarization-Entangled Photon Pairs from a Semiconductor Quantum Dot Using the Optical Stark Effect

Andreas Muller,[1,*] Wei Fang,[1] John Lawall,[2] and Glenn S. Solomon[1,2,†]

[1]*Joint Quantum Institute, National Institute of Standards and Technology and University of Maryland, Gaithersburg, Maryland, USA*
[2]*Atomic Physics Division, National Institute of Standards and Technology, Gaithersburg, Maryland, USA*

(Received 3 June 2009; published 20 November 2009)

In typical epitaxial quantum dots (QDs) the ideally degenerate optical excitons are energy split, preventing the formation of two-photon entanglement in a biexciton decay. We use an external field, here a continuous-wave laser tuned to the QD in the ac Stark limit, to cancel the splitting and create two-photon entanglement. Quantum-state tomography is used to construct the two-photon density matrix. When the splitting is removed it satisfies well-known entanglement tests. Our approach shows that polarization-entangled photons can be routinely produced in semiconductor nanostructures.

DOI: 10.1103/PhysRevLett.103.217402 PACS numbers: 78.67.Hc, 42.50.Pq, 78.47.−p, 78.55.−m

Entangled photons are an important element in quantum information science [1], for example, in quantum repeaters [2] and quantum cryptography [3], and enable fundamental tests of quantum mechanics. They are frequently generated by nonlinear optical processes in bulk media [4]. Parametric down-conversion, for example, yields a large photon-pair flux [5], but is broadband and subject to Poissonian emission statistics. In contrast, single atoms can provide entangled photons discretely, but require careful trapping and preparation.

Semiconductor quantum dots (QDs) combine advantages of both. Despite comprising tens of thousands of atoms, they feature atomlike coherent optical properties [6] with near transform-limited linewidths in the GHz range at cryogenic temperatures [7]. Furthermore, they can be electrically-gated, and integrated into microcavities for enhanced speed and efficiency, and could lead to chip-based devices delivering entangled photon pairs on demand. A well-researched class of QDs with excellent optical properties is the InAs QD in GaAs. Here quasiparticle states are present, such as the electron-hole exciton state, $|X\rangle$, and the two electron-two hole biexciton state, $|XX\rangle$. In the radiative cascade from $|XX\rangle$, a first photon is emitted during a transition to $|X\rangle$, followed by a second photon emitted during a transition to the ground state, $|0\rangle$. Due to the additional binding energy, E_B, in $|XX\rangle$, the two photons have different wavelengths and can be spectrally separated. Ideally, $|X\rangle$ is twofold degenerate, resulting in two indistinguishable decay paths. Therefore, an entangled state such as the Bell state $|\Psi\rangle = (|H_X H_{XX}\rangle + |V_X V_{XX}\rangle)/\sqrt{2}$ can be produced, where H and V denote horizontal and vertical linear polarizations, as proposed by Benson *et al.* [8]. The biexciton radiative cascade could thus lead to a semiconductor source of triggered entangled photon pairs.

In practice, however, the anisotropic electron-hole exchange interaction causes $|X\rangle$ to energy split into $|X_H\rangle$ and $|X_V\rangle$ states, separated by the fine-structure splitting, Δ_{FS} [9]. As in Fig. 1, a total of four linear polarized transitions contribute to the emission spectrum. For this QD, $\Delta_{\mathrm{FS}}/2\pi = 5.5$ GHz, and the typical full width at half maximum of the individual transitions is $\gamma/2\pi \approx 1$ GHz. Since $\Delta_{\mathrm{FS}} \gg \gamma$, the two decay paths can be distinguished, and entanglement vanishes [10]. The two-photon state is now an incoherent mixture described by the density operator $\hat{\rho} = (|HH\rangle\langle HH| + |VV\rangle\langle VV|)/2$ (omitting X and XX indices). Consequently, with the exception of rare coincidental QD symmetry [11], which can be improved by annealing [12,13], or by applying spectral [14] or temporal [15] filtering, entanglement generation is precluded.

Here we demonstrate that polarization entanglement can be established by externally and selectively tuning the fine structure with a far-detuned optical field. Other proposed approaches in which external fields manipulate the fine-structure splitting have used magnetic fields [16], dc electric fields [17], or stress [18], but have not yet shown successful creation of entanglement.

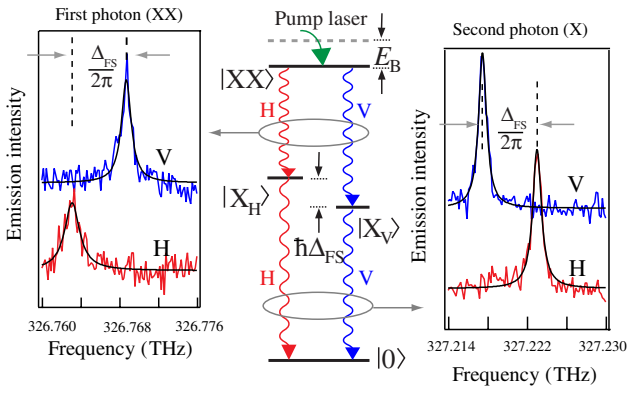

FIG. 1 (color online). Single QD emission spectrum. The biexcitonic (excitonic) transitions give rise to the left (right) spectrum. The two doublets are spectrally separated by $E_B/2\pi\hbar \approx 460$ GHz ($\Delta\lambda \approx 1.3$ nm).

A strong continuous-wave (cw) laser near resonance with an optical transition "dresses" the electronic states, forming pairs of states separated by $\sqrt{\Omega^2 + \delta^2}$, where Ω is the Rabi frequency, and δ the laser detuning from resonance [19]. Because Ω is proportional to the electric field amplitude of the laser, the dressed states separate in frequency with increasing intensity. If Ω is larger than the transition linewidth, the single QD dressed state splitting can be observed *via* the Autler-Townes effect as a doublet, or resonantly as a triplet [7,20–23]. Alternatively, by fixing the laser intensity and detuning the laser, the system undergoes an anticrossing, and the spectrum asymptotically approaches the unperturbed spectrum for $|\delta| \to \infty$. In the asymptotic limit the residual finite offset, the ac Stark shift, represents a small correction to the natural resonance frequency.

The selectivity of dressing specific states and the ability to manipulate these states with the laser intensity (Ω) and detuning (δ) provides a technique to tailor QD energy states precisely. With this approach we can always find a value for δ (given Ω) at which the fine-structure splitting has vanished and where the residual transition in the other dressed state branch is small [22]. We make use of this shift to precisely tailor QD energy states.

The cw laser is applied to the $|X_H\rangle \to |XX\rangle$ transition of Fig. 1. The optical field dresses the $|XX\rangle$ and $|X_H\rangle$ states, resulting in an anticrossing in $|XX\rangle \to |X_H\rangle$, $|XX\rangle \to |X_V\rangle$ and $|X_H\rangle \to |0\rangle$ transitions. Because the laser does not couple to V polarized transitions, the $|X_V\rangle \to |0\rangle$ transition remains unchanged. As depicted in Fig. 2(a), the laser is coupled into the waveguide mode of a planar optical microcavity. The structure serves the dual purpose of allowing improved sample-normal photon extraction from the QD *via* the microcavity, and reduced background laser scattering *via* good orthogonal (in-plane) laser coupling. It contains two distributed Bragg reflectors of alternate quarter-wave layers of GaAs and AlAs above (10 pairs) and beneath (15.5 pairs) a 4λ-thick center spacer defining the cavity. $\lambda = 915$ nm is the resonant wavelength. A QD centered in the cavity interacts with a near-resonant cw laser launched into a lateral waveguide-mode. The near-resonant tuning laser, a Ti-sapphire ring oscillator with a linewidth <1 MHz, is fiber coupled and the fiber rigidly bonded to the cleaved sample edge [7]. The laser is H polarized with frequency ω, and detuned from the $|X_H\rangle \leftrightarrow |XX\rangle$ transition frequency, ω_0 by $\delta/2\pi = \omega_0 - \omega = 25.5$ GHz [Fig. 2(b)]. To pump the biexcitonic state, we apply a second, picosecond pulsed laser (76 MHz repetition period) at 790 nm. It nonresonantly generates carriers in the semiconductor matrix which are subsequently captured in the QD; it is thus probabilistic state initialization. The laser intensity was chosen such that biexciton states were significantly populated. All measurements were taken at 4.2 K in a He-bath cyrostat using a fiber-coupled microscope objective.

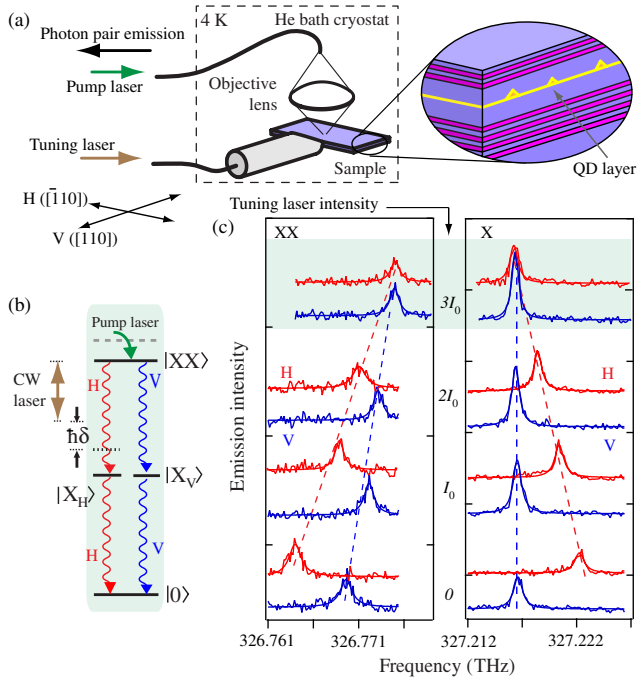

FIG. 2 (color online). (a) Experimental setup. (b) Energy diagram in the presence of the near-resonant tuning laser. (c) Spectra of the evolution of the exciton (left) and biexciton (right) transitions with increasing tuning laser intensity, I. When $I = 3I_0$ (uppermost spectra), the overlapped configuration sketched in (b) is achieved. $I_0 = \Omega/2\pi \approx 8.3$ GHz.

The evolution of the QD emission spectrum with varying tuning laser intensity is shown in Fig. 2(c) for biexciton (left) and exciton (right) transitions at a fixed detuning of $\delta/2\pi = 25.5$ GHz. The laser intensity, and thus Ω, was increased to tune the fine structure until overlap was achieved (uppermost spectra) for $\Omega/2\pi = 25$ GHz. With increasing laser intensity, the $|XX\rangle \to |X_V\rangle$ and $|X_H\rangle \to |0\rangle$ transitions shift with near equal rates, while $|XX\rangle \to |X_H\rangle$ shifts faster and $|X_V\rangle \to |0\rangle$ is stationary. With the degeneracy restored, which-path information appears to be erased and photon entanglement from the $|XX\rangle$ and $|X\rangle$ decay created.

Conclusively establishing the formation of an entangled state requires reconstructing the two-photon density matrix, $\hat{\rho}$ [24]; it contains all the information about the two-photon state. For this purpose, correlation measurements between the biexciton and exciton photons were performed. In the correlation measurements, the collected emission was first divided equally by a nonpolarizing beam splitter into two independent measurement branches. The photons in each branch were then passed through a set of variable retarders and a polarizer for projection into any desired polarization state. Monochromators spectrally selected the exciton emission on one branch and the biexciton emission on the other branch, before single-photon counting avalanche photodiodes detected the signal. Time correlated single-photon counting and histogramming yielded cross-correlation functions $g_{ij}^{(2)}(\tau)$ between

polarizations i and j. Using these correlation measurements, quantum-state tomography was applied to reconstruct the two-photon density matrix $\hat{\rho}$ after [24]. The two-photon density matrix $\hat{\rho}$ was obtained through the relation $\hat{\rho} = (\sum_{\nu=1}^{16} \hat{M}_\nu n_\nu)/(\sum_{\nu=1}^{4} n_\nu)$ derived in Ref. [24], where $\hat{M}_\nu$ denote 16 measurement matrices that depend on a set of 16 tomographic states, and where n_ν is the number of coincidence events. We use the same set as in Ref. [24], chosen to be tomographically complete.

The real and imaginary parts of the density matrix, $\hat{\rho}$, are shown in Fig. 3 for two different conditions. In the absence of any tuning laser [Fig. 3(a)], it has only diagonal elements and represents a state in which the polarization of the two photons are classically correlated, but not entangled [10]. However, when degeneracy has been restored [Fig. 3(b)], $\hat{\rho}$ acquires off-diagonal elements (arrows) associated with an entangled state like $|\Psi\rangle$ above. $\hat{\rho}$ in Fig. 3(b) differs from the ideal matrix $\hat{\rho} = |\Psi\rangle\langle\Psi|$ with corner diagonal elements equal to $1/2$. If it is entangled, it is not maximally entangled. We find that well-known tests, such as the concurrence, tangle, and entanglement of formation tests [24], as well as the Peres criterium [25], are all satisfied for $\hat{\rho}$ of Fig. 3(b) and thus the two-photon state is polarization entangled. They are not satisfied for $\hat{\rho}$ of Fig. 3(a) (Table I). In Fig. 3(b), $\hat{\rho}_{HHVV}$ and $\hat{\rho}_{VVHH}$ have imaginary components, implying that the entangled state obtained is not exactly the state Ψ, as defined above, but rather $|\Psi'\rangle = (|H_X H_{XX}\rangle + \exp[i\theta]|V_X V_{XX}\rangle)/\sqrt{2}$ which differs from Ψ by a phase delay between H and V. This phase delay is partially due to a reflection at our beam splitter, and partially due to imperfect overlap conditions [15].

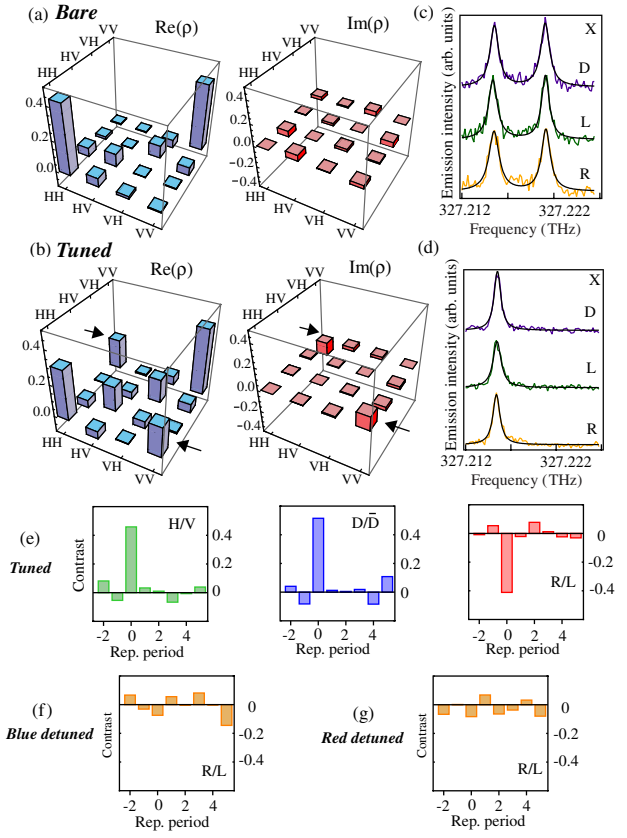

FIG. 3 (color online). (a) Real and imaginary parts of the two-photon density matrix, tomographically reconstructed from 16 coincidence measurements. No tuning laser is applied. (b) Same as in (a), but with a near-resonant laser that creates fine-structure overlap as in Fig. 2(c). Off-diagonal matrix elements appear and the state is now inseparable (entangled). (c) Spectra of exciton emission with detection set to D (diagonal), L (left-circular), and R (right-circular) polarizations, without tuning laser. (d) Same as in (c), but with the tuning laser adjusted to create fine-structure overlap, as in (b). (e) Correlation contrast in different polarization bases under tuned condition as in (b) and (d). Correlation contrast in R/L basis under blue (f) and red (g) detuned conditions, i.e., when the laser does not create fine-structure overlap.

Figures 3(e)–3(g) shows the measured correlation contrast in three different polarization bases, H/V, $D/\bar{D}$, and R/L. The contrast is defined as the difference between copolarized and counterpolarized correlations divided by their sum, and is indexed by repetition period ($\tau_{\text{rep}} = 13.2$ ns). Figure 3(e) corresponds to tuned conditions [Fig. 3(b)]. In Figs. 3(f) and 3(g) the same contrast is shown when there is no fine-structure overlap. This verifies that the R/L contrast, which is needed for entanglement, is only present in optimal overlap conditions.

There are several intrinsic and extrinsic contributions which reduce the photon entanglement. The Peres criterion says that the state is inseparable if the partial transpose of $\hat{\rho}$ has a nonpositive eigenvalue; it is satisfied in our systems if $\rho_{HH,VV}\rho_{VV,HH} > \rho_{HV,HV}\rho_{VH,VH}$ [25]. It is satisfied for the density matrix in Fig. 3(b). However, since the unmodified $\hat{\rho}$ already contains nonzero $\rho_{HV,HV}$ and $\rho_{VH,VH}$ elements, a maximally entangled state cannot be created from it by simply removing Δ_{FS} [26]. To emphasize that coherent control can be successfully used in a wide variety of QDs, we have chosen a QD with the largest splitting encountered in our sample (5.5 GHz). To remove this large splitting, the required Rabi frequencies are large enough so that the condition $\delta \gg \Omega$ breaks down. This results in a residual transition in the second branch of the $|X\rangle$ avoided crossing spectrum that may not be negligible, and would be another cause of diminished entanglement. Finally, residual background light contributes noise, for example, in the off-diagonal elements in Fig. 3(a), which reduces the measured entanglement.

These conclusions are supported by data from another QD (QD2) with smaller initial $\Delta_{\text{FS}} = 2$ GHz for which entanglement qualifiers are much larger. Spectra and the corresponding density matrix for this QD are shown in Fig. 4 for various tuning conditions. In the absence of any near-resonant external laser, the density matrix already measures a very small amount of entanglement because of partial overlap between fine-structure states. This entanglement significantly increases when tuning is applied [Fig. 4(b)]. Here $\Omega/2\pi = 16$ GHz and $\delta/2\pi = -30$ GHz. In Fig. 4(c) the fine-structure splitting is pur-

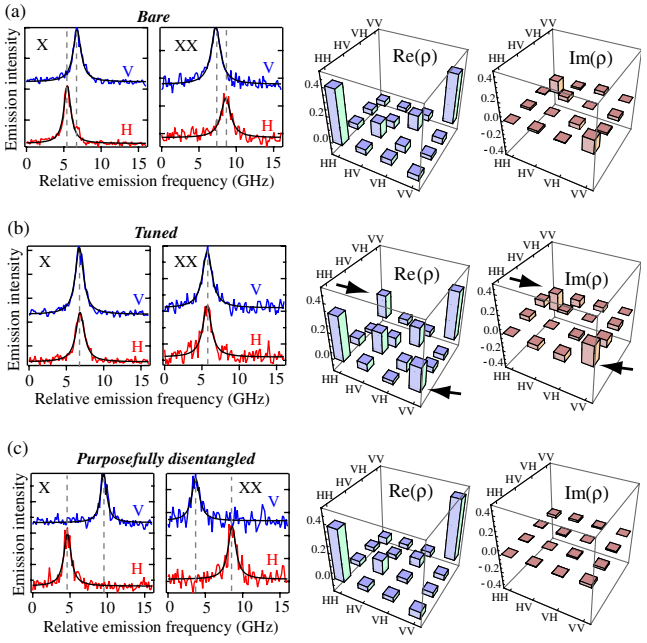

FIG. 4 (color online). QD spectra and density matrices for QD2 under different tuning conditions. (a) Without any applied near-resonant laser. (b) With a laser that creates conditions of spectral overlap. (c) With a laser that purposefully increases the fine structure splitting by reversing the polarity of the laser detuning.

posefully increased by detuning the near-resonant laser in the opposite direction from the resonance condition used in Fig. 4(a) ($\delta/2\pi = +57$ GHz). As anticipated, the off-diagonal matrix elements of ρ disappear completely. Table I summarizes the result of entanglement test for both QD1 and QD2 in the conditions shown. In general, we note that the degree of entanglement could be improved by further increasing δ and Ω. Besides increasing the laser power, improved coupling efficiency into the cavity waveguide will also increase Ω. Furthermore, increasing the transition dipole moment through crystal growth or changing the field strength by cavity effects are additional routes.

In conclusion, we have shown how a near-resonant optical field can be used to selectively tailor QD states. In particular, we have successfully cancelled the exciton fine-structure splitting in a single QD. With which-path information removed, photon entanglement from the QD biexciton-exciton radiative decay was created. Our experiments establish a deterministic scheme that does not require QD preselection, overcoming a main drawback of strain-induced QDs—those in general use—for entangled photon generation. Our approach, which is completely noninvasive, uses a rigid fiber-coupled device and could lead to a compact, on-demand semiconductor source of entangled photons. It also opens new experimental possibilities in tailoring of quantum states and symmetries in QDs, and perhaps between different QDs.

TABLE I. Summary of entanglement tests.

$\Delta_{FS}/2\pi$		Concurrence[a]	Peres Crit[b]	Entangle Form[c]
QD1	bare	0[d]	+0.03	0
5.5 GHz	tuned	0.16 ± 0.05	−0.08	0.06
QD2	bare	0.09 ± 0.03	−0.04	0.02
2.0 GHz	tuned	0.32 ± 0.03	−0.16	0.17
	detuned	0	+0.04	0

[a]See [24].
[b]Smallest eigenvalue of the partial transpose of ρ [25].
[c]Entanglement of formation [24].
[d]Error margins refer to 1 standard deviation.

We acknowledge NSF support through the PFC@JQI.

*andreas.muller@nist.gov
†glenn.solomon@nist.gov

[1] A. Aspect, P. Grangier, and G. Roger, Phys. Rev. Lett. **49**, 91 (1982).
[2] H.-J. Briegel, W. Dür, J. I. Cirac, and P. Zoller, Phys. Rev. Lett. **81**, 5932 (1998).
[3] A. K. Ekert, Phys. Rev. Lett. **67**, 661 (1991).
[4] T. E. Kiess, Y. H. Shih, A. V. Sergienko, and C. O. Alley, Phys. Rev. Lett. **71**, 3893 (1993).
[5] P. G. Kwiat *et al.*, Phys. Rev. Lett. **75**, 4337 (1995).
[6] M. Bayer *et al.*, Nature (London) **405**, 923 (2000).
[7] A. Muller, W. Fang, J. Lawall, and G. S. Solomon, Phys. Rev. Lett. **101**, 027401 (2008).
[8] O. Benson, C. Santori, M. Pelton, and Y. Yamamoto, Phys. Rev. Lett. **84**, 2513 (2000).
[9] D. Gammon, E. S. Snow, B. V. Shanabrook, D. S. Katzer, and D. Park, Phys. Rev. Lett. **76**, 3005 (1996); M. Bayer *et al.*, Phys. Rev. B **65**, 195315 (2002).
[10] C. Santori, D. Fattal, M. Pelton, G. S. Solomon, and Y. Yamamoto, Phys. Rev. B **66**, 045308 (2002).
[11] R. J. Young *et al.*, New J. Phys. **8**, 29 (2006); R. Hafenbrak *et al.*, New J. Phys. **9**, 315 (2007).
[12] W. Langbein *et al.*, Phys. Rev. B **69**, 161301(R) (2004).
[13] R. J. Young *et al.*, Phys. Rev. B **72**, 113305 (2005).
[14] N. Akopian *et al.*, Phys. Rev. Lett. **96**, 130501 (2006).
[15] R. M. Stevenson *et al.*, Phys. Rev. Lett. **101**, 170501 (2008).
[16] R. M. Stevenson *et al.*, Nature (London) **439**, 179 (2006).
[17] K. Kowalik *et al.*, Appl. Phys. Lett. **86**, 041907 (2005); M. M. Vogel *et al.*, Appl. Phys. Lett. **91**, 051904 (2007); B. D. Gerardot *et al.*, Appl. Phys. Lett. **90**, 041101 (2007).
[18] S. Seidl *et al.*, Appl. Phys. Lett. **88**, 203113 (2006).
[19] C. Cohen-Tannoudji, J. Dupont-Roc, and G. Grynberg, *Atom-Photon Interactions* (John Wiley and Sons, New York, 1992).
[20] X. Xu *et al.*, Science **317**, 929 (2007).
[21] A. Muller *et al.*, Phys. Rev. Lett. **99**, 187402 (2007).
[22] G. Jundt, L. Robledo, A. Högele, S. Fält, and A. Imamoglu, Phys. Rev. Lett. **100**, 177401 (2008).
[23] E. B. Flagg *et al.*, Nature Phys. **5**, 203 (2009); A. N. Vamivakas, Y. Zhao, C.-Y. Lu, and M. Atatüre, Nature Phys. **5**, 198 (2009).
[24] D. F. V. James *et al.*, Phys. Rev. A **64**, 052312 (2001).
[25] A. Peres, Phys. Rev. Lett. **77**, 1413 (1996).
[26] A. J. Hudson *et al.*, Phys. Rev. Lett. **99**, 266802 (2007).